AIAA JOURNAL
Vol. 42, No. 10, October 2004

Data Recovery Methodologies for Reduced Dynamic Substructure Models with Internal Loads

Sebastiaan H. J. A. Fransen*
ESA, 2200 AG Noordwijk, The Netherlands

An important step in the design and verification process of spacecraft structures is the coupled dynamic analysis with the launch vehicle in the low-frequency domain. To reduce the costs of computation, the spacecraft and launcher models are dynamically reduced. The recovery of physical responses from the reduced system solution by means of the mode displacement method can be improved by using the mode acceleration method, which accounts for the effect of modal truncation. A further improvement can be obtained by the application of the modal truncation augmentation method, which augments the reduction transformation matrix with a set of pseudoeigenvectors. A drawback of this method is the high number of pseudoeigenvectors for substructure models with a high number of degrees of freedom at the interface. To overcome this problem a solution is provided to reduce the number of pseudoeigenvectors. The aforementioned recovery methods will be compared with regards to the obtained accuracy, specifically for substructure models with applied loads at the internal degrees of freedom (internal loads). For this purpose, the modal truncation augmentation method is further refined by using additional pseudoeigenvectors associated with the internal loads. It is shown that the accuracy obtained with the modal truncation augmentation method is superior to the other recovery methods, whereas the recovery equations remain as simple as possible.

Nomenclature

B	=	reduced number of pseudoeigenvectors associated with interface excitation
dy	=	y displacement
dz	=	z displacement
F	=	matrix of internal load vectors
$\boldsymbol{F}$	=	excitation force vector, internal load vector
G	=	flexibility matrix
I	=	total number of internal degrees of freedom (DOF)
J	=	total number of interface DOF
K	=	stiffness matrix, number of static internal load vectors
M	=	mass matrix
N	=	total number of pseudoeigenvectors, $J + K$
P	=	matrix of total internal load vectors, total number of retained normal modes
$\boldsymbol{P}$	=	total internal load vectors
$\boldsymbol{q}$	=	generalized displacement vector
$\boldsymbol{R}$	=	connection force vector
$\boldsymbol{x}$	=	displacement vector
y, z	=	displacement coordinates
$\boldsymbol{\alpha}$	=	time function vector
β	=	generalized damping matrix
γ	=	pseudoeigenvectors
$\Delta\sigma$	=	difference in stress
δ	=	eigenfrequency associated with interface reduction
ϵ	=	displacement error
ζ	=	modal damping factor
Λ	=	generalized stiffness matrix
μ	=	eigenvectors associated with orthogonalization of truncated static displacement vectors
σ	=	stress
ϕ	=	constraint modes
φ	=	fixed-interface normal modes
χ	=	truncated static displacement vectors, free eigenvectors of Guyan[13] reduced interface
Ψ	=	Craig–Bampton[2] transformation matrix
Ω	=	forcing function frequency
ω	=	eigenfrequency of fixed-interface normal mode or pseudomode

Subscripts

b	=	free eigenvectors of Guyan[13] reduced interface
CB	=	Craig–Bampton[2] model
d	=	deleted modes
FE	=	finite element model
i	=	internal DOF
j	=	interface DOF
k	=	internal load vectors
MA	=	mode acceleration method
MD	=	mode displacement method
MTA	=	modal truncation augmentation method
n	=	pseudoeigenvectors
p	=	fixed-interface normal modes
t	=	truncation value

Superscripts

(cor)	=	correction
T	=	transpose
-1	=	inverse

I. Introduction

THE fixed-interface dynamic reduction method for finite element (FE) models, first proposed by Hurty[1] and further refined by Craig and Bampton[2] (CB) to the CB method, is widely employed. For reduced dynamic models of spacecraft, as used in coupled loads analyses, the classical mode displacement (MD) and mode acceleration (MA) methods[3–6] are usually adopted to recover the responses inside the spacecraft FE model.[7] The MA method adds a static correction to account for modal truncation. More recently, attention has been paid to the modal truncation augmentation (MTA) method,[8–10] which supplements the CB constraint modes and fixed-interface normal modes with a set of pseudoeigenvectors. Earlier, MacNeal[11] and Rubin[12] formed the basic ideas for augmenting the modal basis with pseudoeigenvectors for free-interface dynamic reduction methods.

Presented as Paper 2003-1587 at the AIAA/ASME/ASCE/AHS/ASC 44th Structures, Structural Dynamics, and Materials Conference, Norfolk, VA, 7–10 April 2003; received 1 November 2003; revision received 21 March 2004; accepted for publication 15 April 2004. Copyright © 2004 by Sebastiaan H. J. A. Fransen. Published by the American Institute of Aeronautics and Astronautics, Inc., with permission. Copies of this paper may be made for personal or internal use, on condition that the copier pay the $10.00 per-copy fee to the Copyright Clearance Center, Inc., 222 Rosewood Drive, Danvers, MA 01923; include the code 0001-1452/04 $10.00 in correspondence with the CCC.

*Consultant, Structures Section, AOES Group B.V.; bas.fransen@aoes.com. Professional Member AIAA.

In this paper the MD method, the MA method, and the MTA method will be compared. The differences in terms of procedure will be outlined, as well as the differences in terms of the obtained accuracy. In all cases, the methods will be specifically worked out and tested for substructure models with loads at the internal degrees of freedom (DOF), hereafter called internal loads. Usually the MTA method is applied to substructures without internal loads.[9] In this paper, the usual set of pseudoeigenvectors associated with the interface excitation is extended with a set of pseudoeigenvectors associated with the internal loads. To the author's knowledge, such an approach has not been proposed before in papers on MTA methods in relation to component mode synthesis. In addition, a new method will be proposed to reduce the number of pseudoeigenvectors when adopting the MTA method to substructure models with a high number of DOF at the interface. Instead of rigid-body modes associated with the interface DOF,[9] the free-interface modes of the Guyan[13] reduced component model will be used. The effects on the obtained accuracy, of the new aspects introduced in the MTA method, will be analyzed. Because the emphasis in this paper is on the accuracy of the various recovery methods, output transformation matrices (OTMs) will only be derived for the recovery of accelerations and displacements. Related OTMs can be derived for the recovery of displacement-related responses, such as element stresses, element forces, and forces due to multipoint constraints, as shown by Fransen[6] for substructures without internal loads.

The organization of the paper is as follows: First the CB method is briefly reviewed in Sec. II. In Sec. III, the MD method is explained, followed by the MA method in Sec. IV. Next, in Sec. V, the MTA method is discussed. Section VI is devoted to the damping of the pseudoeigenvectors. In Sec. VII, a method is discussed to reduce the number of pseudoeigenvectors for substructures with a high number of DOF at the interface. The next sections treat a few example problems to demonstrate the methods outlined in the earlier sections. In Sec. VIII a simple beam problem is treated, and in Sec. IX, accuracy aspects for equal cost of computation are dealt with. In Sec. X, the methods are applied to a transient coupled dynamic analysis that simulates a launcher–spacecraft liftoff flight event. Finally, in Sec. XI, conclusions are drawn.

II. CB Reduction

Consider a substructure having J interface DOF and I internal DOF. The substructure is excited both at the interface DOFs by the forces $\boldsymbol{F}_j$ as well as at the internal DOF by the forces $\boldsymbol{F}_i$. The equations of motion for the substructure can be written as follows in partitioned format:

$$\begin{bmatrix} M_{jj} & M_{ji} \\ M_{ij} & M_{ii} \end{bmatrix} \begin{Bmatrix} \ddot{\boldsymbol{x}}_j \\ \ddot{\boldsymbol{x}}_i \end{Bmatrix} + \begin{bmatrix} K_{jj} & K_{ji} \\ K_{ij} & K_{ii} \end{bmatrix} \begin{Bmatrix} \boldsymbol{x}_j \\ \boldsymbol{x}_i \end{Bmatrix} = \begin{Bmatrix} \boldsymbol{F}_j \\ \boldsymbol{F}_i \end{Bmatrix} + \begin{Bmatrix} \boldsymbol{R}_j \\ \boldsymbol{0}_i \end{Bmatrix} \quad (1)$$

The connecting forces $\boldsymbol{R}_j$ cancel out after assembly of the substructures. Damping has not been considered for reasons of simplicity. One can reduce the model dynamically by using a set of P fixed-interface normal modes and J constraint modes to describe the displacement DOF of the FE model (hereinafter called the physical displacements or physical solution). The coordinate transformation procedure according to Craig and Bampton[2] is given by

$$\begin{Bmatrix} \boldsymbol{x}_j \\ \boldsymbol{x}_i \end{Bmatrix} = \Psi \begin{Bmatrix} \boldsymbol{x}_j \\ \boldsymbol{q}_p \end{Bmatrix} \quad (2)$$

where

$$\Psi = \begin{bmatrix} I_{jj} & 0_{jp} \\ \phi_{ij} & \varphi_{ip} \end{bmatrix} \quad (3)$$

In Eq. (3) ϕ_{ij} are the constraint modes due to unit displacements of the interface DOF and φ_{ip} are the fixed-interface normal modes. The constraint modes, also known from static or Guyan[13] reduction, are calculated from the following static equilibrium equation:

$$K_{ij} I_{jj} + K_{ii} \phi_{ij} = 0 \quad (4)$$

or

$$\phi_{ij} = -K_{ii}^{-1} K_{ij} \quad (5)$$

The fixed-interface normal modes are calculated from the following eigenvalue problem:

$$\left[-\omega^2 M_{ii} + K_{ii} \right] \varphi_{ii} = 0 \quad (6)$$

The solution of this eigenvalue problem has I eigenvalues ω^2 and a set of I eigenvectors φ_{ii}. As such φ_{ip} is a subset of the total modal basis of eigenvectors φ_{ii}. Substitution of Eq. (2) into Eq. (1) and premultiplication of Eq. (1) with the transpose of the transformation matrix Ψ gives the following reduced set of equations of motion:

$$\begin{bmatrix} \bar{M}_{jj} & M_{jp} \\ M_{pj} & m_{pp} \end{bmatrix} \begin{Bmatrix} \ddot{\boldsymbol{x}}_j \\ \ddot{\boldsymbol{q}}_p \end{Bmatrix} + \begin{bmatrix} \bar{K}_{jj} & 0_{jp} \\ 0_{pj} & \Lambda_{pp} \end{bmatrix} \begin{Bmatrix} \boldsymbol{x}_j \\ \boldsymbol{q}_p \end{Bmatrix} = \begin{Bmatrix} \boldsymbol{F}_j + \phi_{ij}^T \boldsymbol{F}_i \\ \varphi_{ip}^T \boldsymbol{F}_i \end{Bmatrix} + \begin{Bmatrix} \boldsymbol{R}_j \\ \boldsymbol{0}_p \end{Bmatrix} \quad (7)$$

Solving this set of equations gives the generalized solution in terms of interface DOF and modal DOF. Substitution of the CB solution into Eq. (2) yields the physical solution according to the MD method. Because $(I–P)$ modes have been truncated, such a recovered solution is an approximation of the true solution. However, a contribution of the truncated high-frequency modes is partially accounted for by the constraint modes, which are based on the full stiffness matrix. Hence, the error in the internal displacements $\boldsymbol{x}_i = \phi_{ij} \boldsymbol{x}_j + \varphi_{ip} \boldsymbol{q}_p$ is introduced in the dynamic part and not in the static part of the solution.

For the mass matrix partitions in Eq. (7), the following relations hold:

$$\bar{M}_{jj} = M_{jj} + M_{ji} \phi_{ij} + \phi_{ij}^T M_{ij} + \phi_{ij}^T M_{ii} \phi_{ij} \quad (8)$$

$$M_{jp} = M_{ji} \varphi_{ip} + \phi_{ij}^T M_{ii} \varphi_{ip} \quad (9)$$

When mass normalized modes are assumed,

$$m_{pp} = \varphi_{ip}^T M_{ii} \varphi_{ip} = I_{pp} \quad (10)$$

For the stiffness matrix partitions in Eq. (7), the following relations can be derived:

$$\bar{K}_{jj} = K_{jj} + K_{ji} \phi_{ij} \quad (11)$$

Again when mass normalized modes are assumed,

$$\Lambda_{pp} = \varphi_{ip}^T K_{ii} \varphi_{ip} = \operatorname{diag}\left(\omega_p^2\right) \quad (12)$$

III. MD Method

The recovery of physical displacements according to the MD method is simply accomplished by Eq. (2), which can also be written as

$$\begin{Bmatrix} \boldsymbol{x}_j \\ \boldsymbol{x}_i \end{Bmatrix} = \mathrm{DTM} \begin{Bmatrix} \boldsymbol{x}_j \\ \boldsymbol{q}_p \end{Bmatrix} \quad (13)$$

where the displacement transformation matrix (DTM) is given by

$$\mathrm{DTM} = \Psi \quad (14)$$

In this way, the generalized displacement solution will be expanded to the physical displacement solution. The recovery of physical accelerations is accomplished in a similar way:

$$\begin{Bmatrix} \ddot{\boldsymbol{x}}_j \\ \ddot{\boldsymbol{x}}_i \end{Bmatrix} = \mathrm{ATM} \begin{Bmatrix} \ddot{\boldsymbol{x}}_j \\ \ddot{\boldsymbol{q}}_p \end{Bmatrix} \quad (15)$$

where the acceleration transformation matrix (ATM) is given by

$$\mathrm{ATM} = \Psi \quad (16)$$

Usually, the DTM and ATM matrices are row partitions of the complete CB transformation matrix Ψ, corresponding to a set of selected recovery DOF.

IV. MA Method

In the preceding section the OTMs were derived for the recovery of physical displacements and accelerations according to the MD method. Application of the MA method introduces a static correction to the MD method solution, which improves the accuracy. The static correction accounts for the truncated high-frequency modes and will be added during the recovery process, after the completion of the coupled analysis. To derive the OTMs on the basis of the MA method, the physical equations of motion (1) are taken as the starting point. Those equations can be split into two row partitions. The first row partition is given by

$$[M_{jj} \quad M_{ji}] \begin{Bmatrix} \ddot{\boldsymbol{x}}_j \\ \ddot{\boldsymbol{x}}_i \end{Bmatrix} + [K_{jj} \quad K_{ji}] \begin{Bmatrix} \boldsymbol{x}_j \\ \boldsymbol{x}_i \end{Bmatrix} = \boldsymbol{F}_j + \boldsymbol{R}_j \tag{17}$$

From the second row partition the internal displacements $\boldsymbol{x}_i$ can be solved:

$$\boldsymbol{x}_i = \begin{bmatrix} -K_{ii}^{-1}M_{ij} & -K_{ii}^{-1}M_{ii} \end{bmatrix} \begin{Bmatrix} \ddot{\boldsymbol{x}}_j \\ \ddot{\boldsymbol{x}}_i \end{Bmatrix} - K_{ii}^{-1}K_{ij}\boldsymbol{x}_j + K_{ii}^{-1}\boldsymbol{F}_i \tag{18}$$

Equation (18) can be rewritten as follows when the interface DOFs are included in the displacement recovery vector:

$$\begin{Bmatrix} \boldsymbol{x}_j \\ \boldsymbol{x}_i \end{Bmatrix} = \begin{bmatrix} 0_{jj} & 0_{ji} \\ -K_{ii}^{-1}M_{ij} & -K_{ii}^{-1}M_{ii} \end{bmatrix} \begin{Bmatrix} \ddot{\boldsymbol{x}}_j \\ \ddot{\boldsymbol{x}}_i \end{Bmatrix} + \begin{bmatrix} I_{jj} \\ -K_{ii}^{-1}K_{ij} \end{bmatrix} \boldsymbol{x}_j + \begin{bmatrix} 0_{ji} \\ K_{ii}^{-1} \end{bmatrix} \boldsymbol{F}_i \tag{19}$$

Equation (19) expresses the physical displacements as a function of the physical accelerations, interface displacements, and internal forces. This equation will now be used to derive the OTMs needed for the recovery of displacements according to the MA method. Substitution of the second derivative of Eq. (2) into Eq. (19) yields

$$\begin{Bmatrix} \boldsymbol{x}_j \\ \boldsymbol{x}_i \end{Bmatrix} = \mathrm{DTM}_1 \begin{Bmatrix} \ddot{\boldsymbol{x}}_j \\ \ddot{\boldsymbol{q}}_p \end{Bmatrix} + \mathrm{DTM}_2\boldsymbol{x}_j + \mathrm{DTM}_3\boldsymbol{F}_i \tag{20}$$

where

$$\mathrm{DTM}_1 = \begin{bmatrix} 0_{jj} & 0_{jp} \\ -K_{ii}^{-1}(M_{ij} + M_{ii}\phi_{ij}) & -K_{ii}^{-1}M_{ii}\varphi_{ip} \end{bmatrix} \tag{21}$$

$$\mathrm{DTM}_2 = \begin{bmatrix} I_{jj} \\ \phi_{ij} \end{bmatrix} \tag{22}$$

$$\mathrm{DTM}_3 = \begin{bmatrix} 0_{ji} \\ K_{ii}^{-1} \end{bmatrix} \tag{23}$$

To avoid the expensive computation of K_{ii}^{-1} in DTM_3, note that the applied loads $\boldsymbol{F}_i$ can be written as the sum of a set of K spatial load distribution vectors ($K \ll I$) times their corresponding time functions:

$$\boldsymbol{F}_i = \sum_{k=1}^{K} (\tilde{\boldsymbol{F}}_i)_k \alpha_k(t) = \tilde{F}_{ik}\boldsymbol{\alpha}_k \tag{24}$$

Each spatial load distribution vector $(\tilde{\boldsymbol{F}}_i)_k$ in Eq. (24) represents a set of correlated loads applied to the internal DOFs. Such load vectors could be point forces, gravity forces, or pressure forces. Now Eq. (20) can be written as

$$\begin{Bmatrix} \boldsymbol{x}_j \\ \boldsymbol{x}_i \end{Bmatrix} = \mathrm{DTM}_1 \begin{Bmatrix} \ddot{\boldsymbol{x}}_j \\ \ddot{\boldsymbol{q}}_p \end{Bmatrix} + \mathrm{DTM}_2\boldsymbol{x}_j + \mathrm{DTM}_3^*\boldsymbol{\alpha}_k \tag{25}$$

where

$$\mathrm{DTM}_3^* = \begin{bmatrix} 0_{jk} \\ K_{ii}^{-1}\tilde{F}_{ik} \end{bmatrix} \tag{26}$$

The utilization of the MD method recovery procedure is much more user friendly than the MA method recovery procedure, as can be seen by comparison of the number of multiplications executed in Eq. (13) and Eq. (25). However, the MD method is less accurate. A better recovery procedure, more accurate than the MA method and with the simplicity of the MD method, is the MTA method to be discussed in Sec. V.

One could propose to avoid the problem of internal loads by including the internal DOF associated with internal loads in the interface set. However, for problems with a large number of loaded internal DOF, such as for gravity and pressure forces, the number of interface DOF would become too large. In addition it would deteriorate the representativeness of the fixed-interface normal modes, which would be driven toward higher frequencies because the substructure clamped at such an interface becomes highly constrained.

After some elaboration (Appendix), the following equation can be derived from the aforementioned equations, giving the relationship between the physical internal displacements recovered by the MA method and those recovered by the MD method:

$$\boldsymbol{x}_{i\mathrm{MA}} = \boldsymbol{x}_{i\mathrm{MD}} + G_d\left\{\boldsymbol{F}_i - \left[M_{ij} - M_{ii}K_{ii}^{-1}K_{ij}\right]\ddot{\boldsymbol{x}}_j\right\} \tag{27}$$

where the residual flexibility matrix of the truncated modes G_d is given by

$$G_d = \varphi_{id}\Lambda_{dd}^{-1}\varphi_{id}^T = K_{ii}^{-1}\left[I_{ii} - M_{ii}\varphi_{ip}\varphi_{ip}^T\right] \tag{28}$$

The mode set φ_{id} is the truncated mode set. When Eq. (27) is considered, it can be seen that the MA method corrects the MD method for mode truncation by the addition of a static displacement correction. The internal forces shown in the correction term are composed of the applied internal loads and the inertia forces at the internal DOF due to interface excitation.

V. MTA Method

In this section, a brief explanation is given of the MTA method.[8–10] As explained in Sec. IV, the MA method corrects for the effects of mode truncation only at the stage of recovery. The MTA method, however, corrects beforehand by augmenting the modal basis used in the CB transformation matrix with an additional set of N pseudoeigenvectors:

$$\Psi = \begin{bmatrix} I_{jj} & 0_{jp} & 0_{jn} \\ \phi_{ij} & \varphi_{ip} & \gamma_{in} \end{bmatrix} \tag{29}$$

To define a set of N pseudoeigenvectors, which will be independent of the existing set of retained modes, we will consider the MA method static displacement correction as presented in Eq. (27):

$$\boldsymbol{x}_i^{(\mathrm{cor})} = G_d\boldsymbol{P}_i \tag{30}$$

where

$$\boldsymbol{P}_i = \boldsymbol{F}_i - \left[M_{ij} - M_{ii}K_{ii}^{-1}K_{ij}\right]\ddot{\boldsymbol{x}}_j \tag{31}$$

When substituting Eq. (24) for the applied internal loads $\boldsymbol{F}_i$, we can write

$$\boldsymbol{P}_i = \left[\tilde{F}_{ik} \;\vdots\; -M_{ij} + M_{ii}K_{ii}^{-1}K_{ij}\right] \begin{Bmatrix} \boldsymbol{\alpha}_k \\ \ddot{\boldsymbol{x}}_j \end{Bmatrix} \tag{32}$$

For unitary interface accelerations and unitary time functions, a set of $N = K + J$ spatial load distribution vectors is obtained:

$$P_{in} = \left[\tilde{F}_{ik} \;\vdots\; M_{ij} - M_{ii}K_{ii}^{-1}K_{ij}\right] \tag{33}$$

Substitution of the load vectors P_{in} into Eq. (30) yields a set of N truncated displacement vectors:

$$\boldsymbol{\chi}_{in} = G_d P_{in} = G_d\left[\tilde{F}_{ik} \;\vdots\; M_{ij} - M_{ii}K_{ii}^{-1}K_{ij}\right] \tag{34}$$

In the study performed by Dickens and Stroeve,[9] the spacecraft substructure was excited at its interface only, whereas in this paper we consider substructures with both interface excitation and excitation at the internal DOF. For this reason, the J load vectors, associated with the interface excitation, are supplemented with K load vectors associated with excitation at the internal DOF ($J+K=N$). The static response $G_d\tilde{F}_{ik}$ can be associated with residual attachment modes for free-interface methods. However, in this paper the interface is constrained, and the forces are applied to the internal DOF rather than to the interface. The static response $G_d[M_{ij}-M_{ii}K_{ii}^{-1}K_{ij}]$ can be associated with residual inertia relief modes, if the interface would be rigid or statically determinate. For the general case of a statically indeterminate flexible interface, the term $G_d[M_{ij}-M_{ii}K_{ii}^{-1}K_{ij}]$ forms a special class of static modes associated with the internal inertia loads due to unit accelerations of each interface DOF while keeping all other interface DOF constrained. In that case, there is no direct relationship with the classical residual inertia relief modes known for free-interface systems.[5,14]

The truncated displacement vectors in Eq. (34) are finally orthogonalized with respect to K_{ii} and M_{ii} by the following reduced eigenvalue problem:

$$M_{nn}=\chi_{in}^T M_{ii}\chi_{in} \tag{35}$$

$$K_{nn}=\chi_{in}^T K_{ii}\chi_{in} \tag{36}$$

$$\left[-\omega^2 M_{nn}+K_{nn}\right]\mu_{nn}=0 \tag{37}$$

where mass normalization is enforced:

$$\mu_{nn}^T M_{nn}\mu_{nn}=I_{nn} \tag{38}$$

Then the mass normalized pseudoeigenvectors can be defined as

$$\gamma_{in}=\chi_{in}\mu_{nn} \tag{39}$$

Note that

$$\gamma_{in}^T M_{ii}\gamma_{in}=\mu_{nn}^T\chi_{in}^T M_{ii}\chi_{in}\mu_{nn}=m_{nn}=I_{nn} \tag{40}$$

$$\gamma_{in}^T K_{ii}\gamma_{in}=\mu_{nn}^T\chi_{in}^T K_{ii}\chi_{in}\mu_{nn}=\Lambda_{nn}=\mathrm{diag}\left(\omega_n^2\right) \tag{41}$$

where ω_n are the pseudoeigenfrequencies associated to the pseudoeigenvectors γ_{in}. The pseudoeigenvectors can be regarded as high-frequency ($\omega_n>\omega_p$) fixed-interface correction modes. The mass normalized pseudoeigenvectors γ_{in} according to Eq. (40) are now consistent with the mass normalized modes φ_{ip}; refer to Eq. (6). In addition, note that the pseudoeigenvectors are orthogonal to the retained modes φ_{ip} with respect to K_{ii} and M_{ii} because they are related to the deleted modes φ_{id}; refer to Eqs. (28) and (34). The augmented CB transformation matrix, as given by Eq. (29), can now be adopted to generate the equations of motion for the reduced dynamic substructure model in the same fashion as explained in Sec. II:

$$\begin{bmatrix}\bar{M}_{jj} & M_{jp} & M_{jn}\\ M_{pj} & m_{pp} & 0_{pn}\\ M_{nj} & 0_{np} & m_{nn}\end{bmatrix}\begin{Bmatrix}\ddot{\boldsymbol{x}}_j\\ \ddot{\boldsymbol{q}}_p\\ \ddot{\boldsymbol{q}}_n\end{Bmatrix}+\begin{bmatrix}\bar{K}_{jj} & 0_{jp} & 0_{jn}\\ 0_{pj} & \Lambda_{pp} & 0_{pn}\\ 0_{nj} & 0_{np} & \Lambda_{nn}\end{bmatrix}\begin{Bmatrix}\boldsymbol{x}_j\\ \boldsymbol{q}_p\\ \boldsymbol{q}_n\end{Bmatrix}$$

$$=\begin{Bmatrix}\boldsymbol{F}_j+\phi_{ij}^T\boldsymbol{F}_i\\ \varphi_{ip}^T\boldsymbol{F}_i\\ \gamma_{in}^T\boldsymbol{F}_i\end{Bmatrix}+\begin{Bmatrix}\boldsymbol{R}_j\\ \boldsymbol{0}_p\\ \boldsymbol{0}_n\end{Bmatrix} \tag{42}$$

Equation (42) shows that the correction modes form a natural extension of the retained normal modes. They are tuned to the internal excitation forces, that is, to the internal loads and inertia loads. Besides a quasistatic correction for low-frequency excitation, they also provide a dynamic correction for the high-frequency excitation. The frequency range Λ_{nn} of the correction modes, which extends the frequency range of the retained normal modes, indicates up to which frequency a dynamic correction is provided. Evidently the correction modes can only be excited if the frequency content of the forcing function partially or completely overlaps with the frequency range of the correction modes.

The recovery of physical responses is now simply accomplished by the employment of the MD method as outlined in Sec. III. This implies that the amount of work associated with the recovery of displacements and displacement-related data is reduced compared to the MA method. For reduced substructure models with internal loads, only one OTM is needed for the recovery of displacements instead of three, as can be deduced by comparison of Eq. (13) and Eq. (25), respectively. This means that with the MTA method a simple and accurate recovery procedure is available. To compute the pseudoeigenvectors, additional computational effort is required, although the effort is small because the computation of the truncated static displacement vectors and the subsequent solving of a reduced N by N eigenvalue problem does not demand a lot of CPU time.

VI. Damping of the MTA Pseudoeigenvectors

In the preceding sections, a discussion on the damping has been omitted because modal damping is usually assigned after having generated the CB-model mass and stiffness matrices. In that case, a diagonal modal damping matrix can be defined, assuming the damping of the interface partition can be neglected. For a CB model where the modal basis has been augmented with N pseudoeigenvectors, the equation of motion of the substructure then takes the following form:

$$\begin{bmatrix}\bar{M}_{jj} & M_{jp} & M_{jn}\\ M_{pj} & m_{pp} & 0_{pn}\\ M_{nj} & 0_{np} & m_{nn}\end{bmatrix}\begin{Bmatrix}\ddot{\boldsymbol{x}}_j\\ \ddot{\boldsymbol{q}}_p\\ \ddot{\boldsymbol{q}}_n\end{Bmatrix}+\begin{bmatrix}\bar{K}_{jj} & 0_{jp} & 0_{jn}\\ 0_{pj} & \Lambda_{pp} & 0_{pn}\\ 0_{nj} & 0_{np} & \Lambda_{nn}\end{bmatrix}\begin{Bmatrix}\boldsymbol{x}_j\\ \boldsymbol{q}_p\\ \boldsymbol{q}_n\end{Bmatrix}$$

$$+\begin{bmatrix}0_{jj} & 0_{jp} & 0_{jn}\\ 0_{pj} & \beta_{pp} & 0_{pn}\\ 0_{nj} & 0_{np} & \beta_{nn}\end{bmatrix}\begin{Bmatrix}\dot{\boldsymbol{x}}_j\\ \dot{\boldsymbol{q}}_p\\ \dot{\boldsymbol{q}}_n\end{Bmatrix}=\begin{Bmatrix}\boldsymbol{F}_j+\phi_{ij}^T\boldsymbol{F}_i\\ \varphi_{ip}^T\boldsymbol{F}_i\\ \gamma_{in}^T\boldsymbol{F}_i\end{Bmatrix}+\begin{Bmatrix}\boldsymbol{R}_j\\ \boldsymbol{0}_p\\ \boldsymbol{0}_n\end{Bmatrix} \tag{43}$$

where for mass normalized modes,

$$\beta_{pp}=\mathrm{diag}(2m_p\omega_p\zeta_p)=\mathrm{diag}(2\omega_p\zeta_p) \tag{44}$$

$$\beta_{nn}=\mathrm{diag}(2m_n\omega_n\zeta_n)=\mathrm{diag}(2\omega_n\zeta_n) \tag{45}$$

As discussed in Sec. V, the pseudoeigenvectors extend the frequency range of the normal modes into a higher frequency range. Hence, it can be seen that the damping levels in the frequency range of the pseudoeigenvectors should be similar to the damping levels that normally would be applied if those modes were normal modes in that frequency range. However, if the substructure model is too course to represent the higher modes adequately, one should consider the application of higher damping levels for the corresponding MTA modes. As already mentioned, the correction modes can only be excited if the frequency content of the forcing function partially or completely overlaps with the frequency range of the correction modes.

VII. Reducing the Number of MTA Pseudoeigenvectors

For substructures with numerous interface DOF (J DOF), it would be advantageous to reduce the number of pseudoeigenvectors, which equates to $N=J+K$. For this purpose, an interface reduction method could be adopted. In this respect rigid interface reduction has been used by Dickens and Stroeve,[9] and flexible interface reduction has been proposed by Rixen.[15] In this paper, the flexible interface reduction method will be utilized for each substructure separately rather than for the whole CB system as proposed by Rixen.[15] In this way, the need for information from neighboring substructures is avoided. The interface reduction method in the true sense, that is, to reduce the number of interface DOF of a CB model, has been proposed and demonstrated by Craig and Chang[16] and has been employed by Tan et al.[17] and Castanier et al.[18]

The interface reduction method can be used to reduce the number of pseudoeigenvectors by changing Eq. (34) as follows:

$$\chi_{in} = G_d\left[\tilde{F}_{ik} \;\vdots\; \left[M_{ij} - M_{ii}K_{ii}^{-1}K_{ij}\right]\chi_{jb}\right] \tag{46}$$

where the interface normal modes χ_{jb} are calculated from the reduced eigenvalue problem defined by the Guyan reduced interface partition of the CB mass and stiffness matrix (modal DOF constrained):

$$\left[-\delta^2\bar{M}_{jj} + \bar{K}_{jj}\right]\chi_{jj} = 0 \tag{47}$$

From Eq. (47), J positive roots can be found and J associated eigenvectors. To reduce the interface, we will use only B eigenvectors, where $B < J$. If there are any rigid-body interface modes (such as for free-launcher substructures), these should always be included in the set of B modes to obtain at least the complete static correction in all rigid-body mode directions. In case of six rigid-body modes, and in case $B = 6$, the concept is related to residual inertia relief modes with a rigid interface. The addition of free-interface flexible modes to the rigid-body modes will include the effect of the interface flexibility in the residual static response (46) and finally in the pseudoeigenvectors (39). In the beam model example of Sec. VII, the difference in the obtained accuracy with flexible-interface reduction as compared to rigid-interface reduction will be demonstrated.

It is the author's experience that at least those free-interface modes should be retained with eigenfrequencies up to the truncation frequency of the CB-model:

$$\delta_t \geq \omega_t \tag{48}$$

In this way the CB/MTA reduction procedure does not require any additional control parameters because the same upper eigenfrequency bound can be used for both of the eigenvalue problems given by Eqs. (6) and (47).

The truncation frequency ω_t should at least be equal to two times the highest frequency Ω_t observed in the forcing functions used to excite the structure. This is generally taken as the rule of thumb for CB models based on fixed-interface modes. However, for CB models enriched with pseudoeigenvectors, a value between 1.0 and 2.0 times Ω_t might be sufficient because the apparent truncation frequency, that is, the highest MTA mode frequency, is much higher than the original truncation frequency of the CB model. This would be an interesting point for further research, but has not been explored in this paper.

VIII. Beam Model

The beam test model is shown in Fig. 1. The model is constituted of simple beam element connections (CBAR[19]) with axial stiffness, shear stiffness, and bending stiffness. The outer two elements, between nodes 300–301 and 400–401, are considered as residual physical structure. The part of the model between nodes 100 and 110 will be subject to CB reduction. The CB model will be connected to the residual structure by means of its interface nodes 100 and 110. Interface node 100 is connected to node 301 and interface node 110 to node 401. In the frequency response analysis, nodes 300 and 400 of the residual structure will be fully constrained. The sinusoidal loads, classified as either internal or interface loads, are indicated in Fig. 1. The modal frequency response analysis is performed in the frequency range of 0.1–10 Hz with a frequency step of 0.1 Hz, retaining all system (CB model plus residual structure) modes. The modal damping in the analysis is set to 1% for all system modes. Note that the damping has not been assigned to the CB model and the residual structure separately because a modal frequency response analysis method was chosen. Hence, the approach is different compared to what has been proposed in Sec. VI, where a direct solution method is assumed for the assembled system.

The modal content of the CB model is intentionally kept small. When employing the MD and MA method, only the first two clamped bending modes are retained, which corresponds to a truncation frequency $\omega_t = 2.0$ Hz. When using the MTA method, 13 additional pseudoeigenvectors can be computed from Eq. (37), $N = K + J = 1 + 12 = 13$. In that case, 13 pseudomodes could be added to the retained basis of two normal modes. The eigenfrequencies of the normal modes (normal/φ_{ip}) and pseudomodes (MTA/γ_{in}) are given in Table 1. One can clearly distinguish between bending modes (same eigenfrequency for in-plane and out-of-plane bending) and axial modes.

In Fig. 2, the displacement response of node 105 in z direction is plotted for the MD, MA, and MTA methods. In addition, the response of node 105 for the FE system (all modes retained) is plotted for comparison. As already mentioned, the MD and MA method response are plotted for a modal basis of two normal modes. Visually the MTA method response coincides with FE-model response. For the MTA method, the response curve is plotted for which all 13 pseudoeigenvectors are employed. (In Fig. 2, MTA/2/1/12 denotes MTA method/2 normal modes/1 MTA vector due to applied internal load/12 MTA vectors due to inertia loads from interface excitation.) Figure 2 shows that both the MD and MA method are not suited for response prediction above the cutoff frequency, whereas the MTA method clearly is. Up to 2 Hz, all methods perform quite reasonably. A more appropriate look at the methods' accuracy is shown in Fig. 3. Here the error is plotted with respect to the FE-model response. The error is defined as follows:

$$\epsilon = \frac{|\mathrm{d}z_{\mathrm{CB}} - \mathrm{d}z_{\mathrm{FE}}|}{|\mathrm{d}z_{\mathrm{FE}}|} \tag{49}$$

Again we note much better accuracy for the MTA method over the entire frequency range. In addition, we see that the MD method performs badly toward 0 Hz (static case) because mode truncation causes an error in the displacement enforced by the static internal load. The static correction of the MA recovery method or the introduction of additional pseudoeigenvectors avoids such a static error. In terms of accuracy, the MTA method clearly outperforms the other two methods. Figure 3 also shows response curves for

Table 1 Eigenfrequencies of fixed-interface normal modes and MTA modes: beam

Mode number	Eigenfrequency, Hz	Mode type
1	1.6	Normal/φ_{i1}
2	1.6	Normal/φ_{i2}
3	4.4	MTA/γ_{i1}
4	4.4	MTA/γ_{i2}
5	8.6	MTA/γ_{i3}
6	8.6	MTA/γ_{i4}
7	15.3	MTA/γ_{i5}
8	15.3	MTA/γ_{i6}
9	15.8	MTA/γ_{i7}
10	21.5	MTA/γ_{i8}
11	22.9	MTA/γ_{i9}
12	31.8	MTA/γ_{i10}
13	36.6	MTA/γ_{i11}
14	116.2	MTA/γ_{i12}
15	233.6	MTA/γ_{i13}

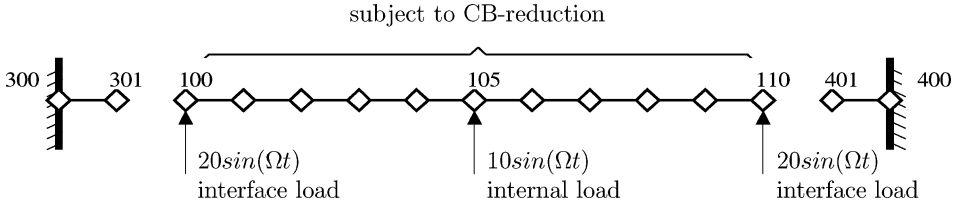

Fig. 1 Beam FE model.

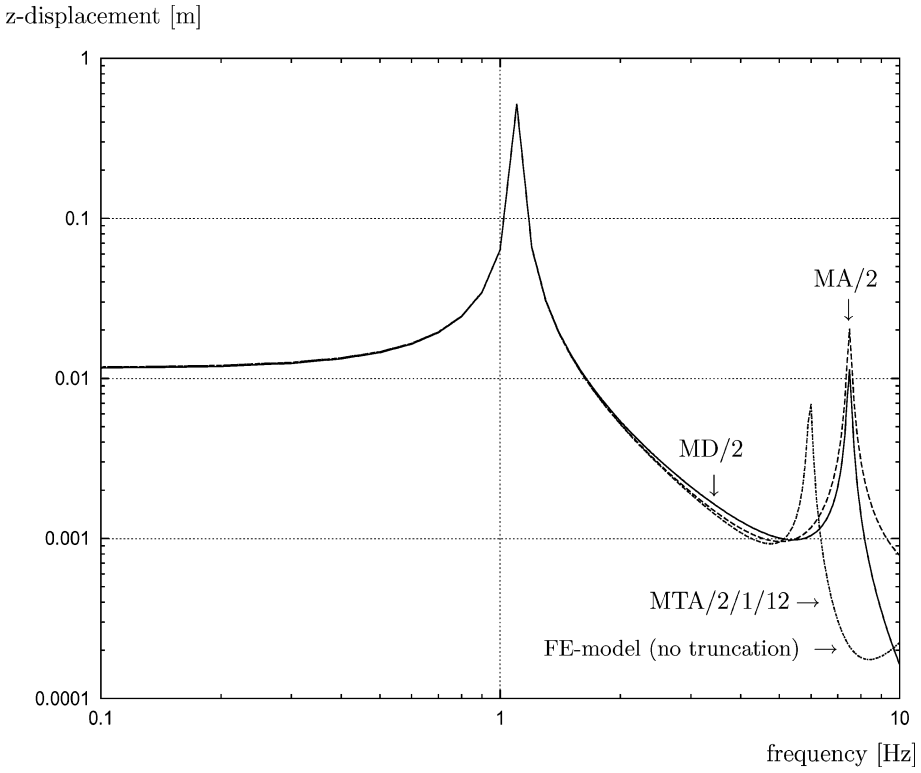

Fig. 2 *Z*-displacement response, node 105, beam.

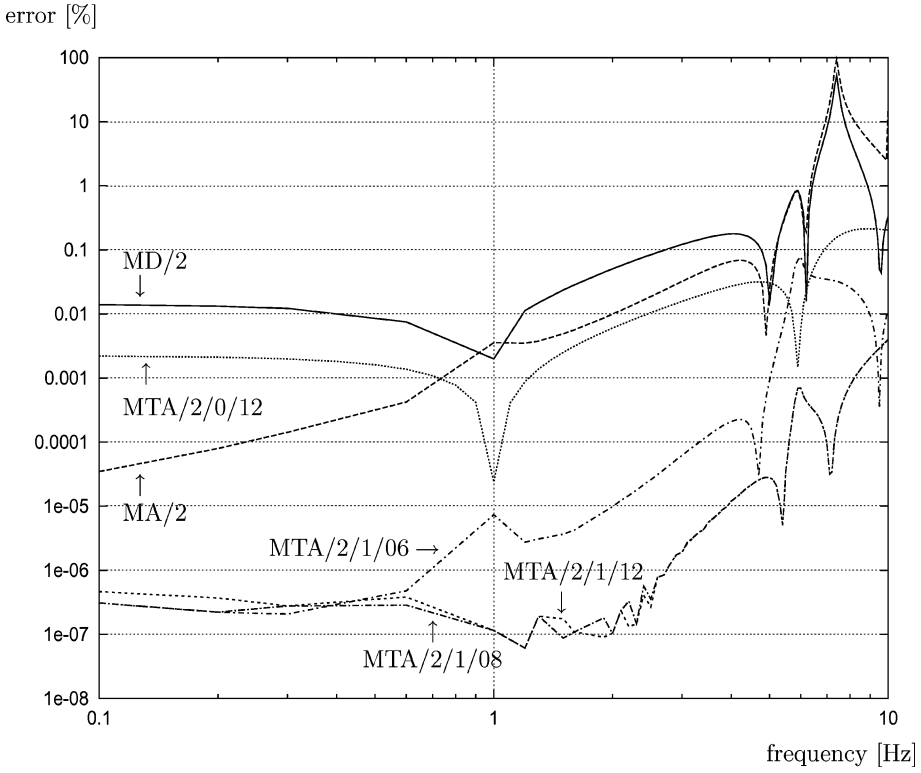

Fig. 3 Error z-displacement response, node 105, beam.

which the number of pseudoeigenvectors included in the CB transformation matrix has been reduced according to the method outlined in Sec. VII. The response labeled MTA/2/1/8 has approximately the same quality as the MTA/2/1/12 response. The response labeled MTA/2/1/6 clearly is less accurate because only the rigid-body modes were used to reduce the number of MTA vectors (rigid interface). In addition, the curve labeled MTA/2/0/12 shows the adverse effect of not including the MTA vector associated with the internal load $\tilde{F}_{ik}$ [refer to Eq. (34)]. For the curve labeled MTA/2/1/6, the eigenfrequencies of the modes and pseudomodes are given in Table 2.

IX. Space Frame Model

A space frame model was employed to compare the MD, MA, and MTA methods for equal size of reduced models. Hence, the cost of computation will be constant throughout the frequency response analyses conducted in this section. The free-space frame FE model

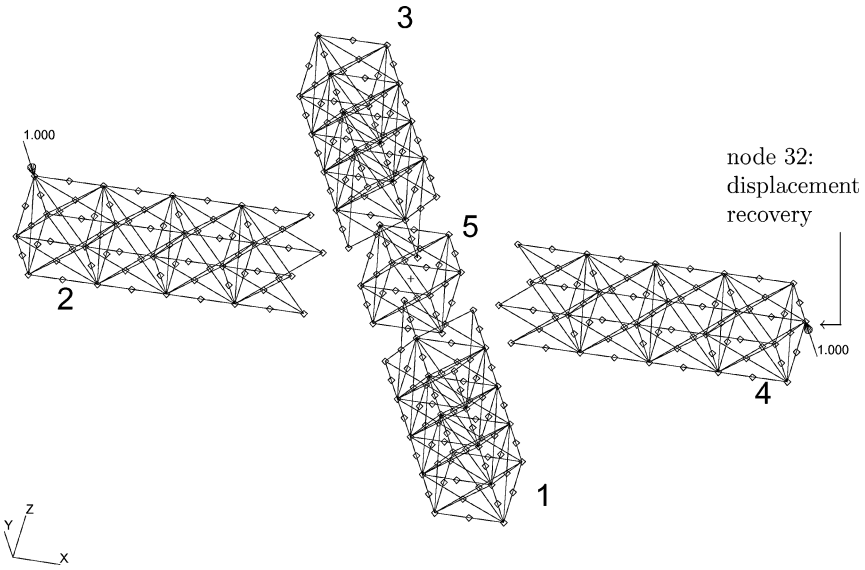

Fig. 4 Space frame substructure FE models.

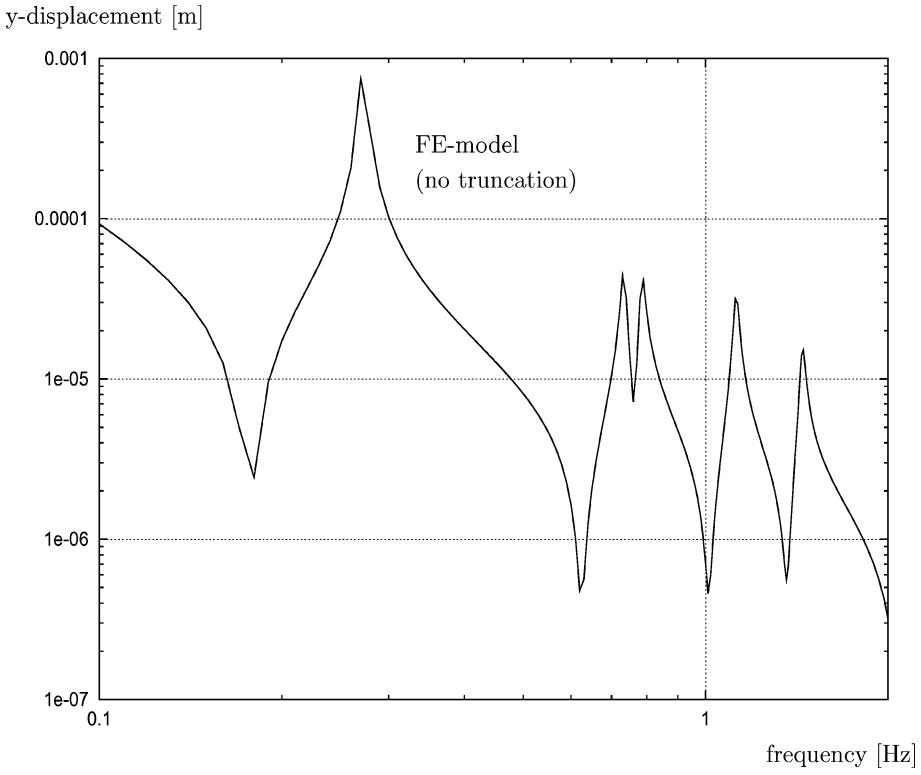

Fig. 5 *Y*-displacement response, node 32, space frame.

Table 2 Eigenfrequencies of fixed-interface normal modes and reduced set of MTA modes: beam

Mode number	Eigenfrequency, Hz	Mode type
1	1.6	Normal/φ_{i1}
2	1.6	Normal/φ_{i2}
3	4.5	MTA/γ_{i1}
4	4.5	MTA/γ_{i2}
5	8.7	MTA/γ_{i3}
6	8.9	MTA/γ_{i4}
7	15.8	MTA/γ_{i5}
8	21.9	MTA/γ_{i6}
9	116.2	MTA/γ_{i7}

was subdivided into five substructures as shown in Fig. 4. The outer substructures were reduced, and the center substructure was used as residual structure. Unit sinusoidal loads will be applied in-phase to substructures 2 and 4 as indicated in Fig. 4. The modal frequency response analysis is performed in the frequency range of 0.1–2.0 Hz with a frequency step of 0.01 Hz, retaining all system (CB models plus residual structure) modes. The modal damping in the analysis is set to 1% for all system modes. Similar to the beam example in Sec. VIII, the damping has not been assigned to the CB models and the residual structure separately because a modal frequency response analysis method was chosen.

A total of 36 modes were used for each substructure, constituting 12 static constraint modes and 24 additional modes. The set

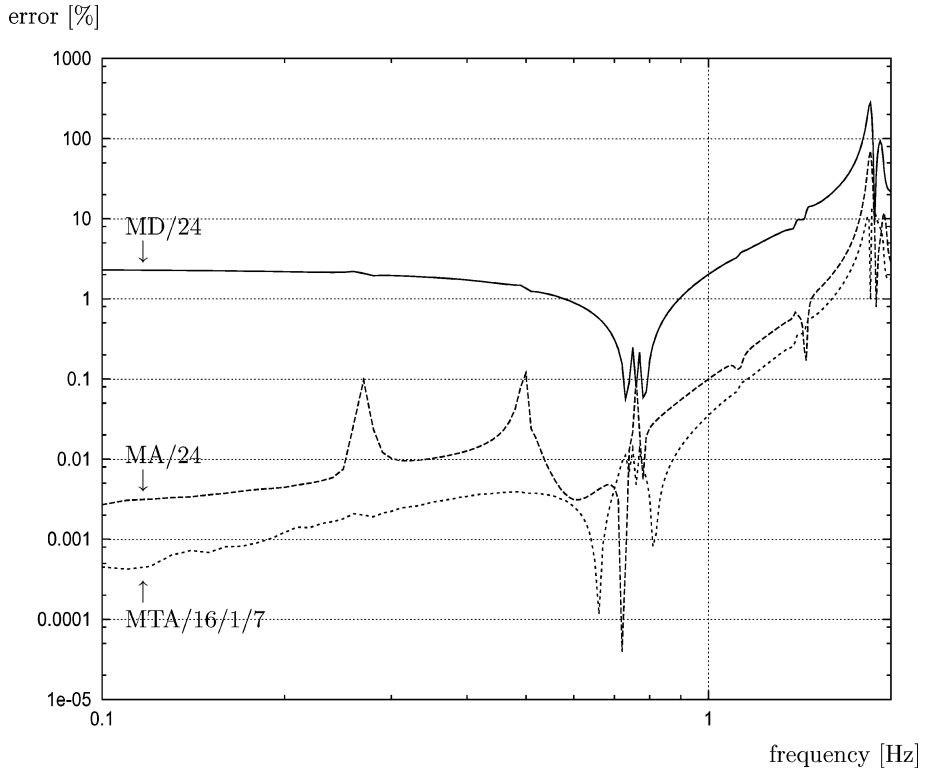

Fig. 6 Error *y*-displacement response, node 32, space frame.

of 24 modes comprises fixed-interface normal modes and pseudo-modes (the latter for MTA method only). Accordingly, the substructure models, containing 120 DOF, were reduced by 70%. For the MD and MA method CB models, the 24 fixed-interface normal modes correspond to a truncation frequency $\omega_t = 5.4$ Hz. For the MTA method CB models, 16 fixed-interface normal modes were retained, which corresponds to a truncation frequency $\omega_t = 4.8$ Hz. When the interface reduction technique as outlined in Sec. VII was used, the number of MTA modes was reduced from $J + K = 12 + 1$ to $B + K = 7 + 1$. The range of the MTA correction modes is 6.1–11.8 Hz. The y-displacement response of internal node 32 of substructure 4 (Fig. 4) was computed for the various methods. The y-displacement response of node 32 for the FE model (no truncation) is shown in Fig. 5. To compare the methods, the error for the y-displacement response is plotted in Fig. 6. The error is defined as follows, with reference, to Eq. (49):

$$\epsilon = \frac{|\mathrm{d}y_{\mathrm{CB}} - \mathrm{d}y_{\mathrm{FE}}|}{|\mathrm{d}y_{\mathrm{FE}}|} \tag{50}$$

Obviously the MA method outperforms the MD method. The MTA method, which is based on fewer fixed-interface normal modes than the MD and MA methods (16 vs 24), is more accurate in the major part of the frequency range. Hence, we can conclude that, for equal analysis cost, the MTA method outperforms the MA method in the major part of the frequency range. At the main system mode at 0.27 Hz, the errors for the MD, MA, and MTA methods amount to 2, 0.1, and 0.002%, respectively. In other words, the error at the main mode for the MA method and MTA method is respectively 20 times and 1000 times smaller than the MD method error.

X. Ariane-5 Dynamic Mathematical Model

The Ariane-5 dynamic mathematical model, subdivided into its substructures, is shown in Fig. 7. The four substructures are the two strap-on boosters (EAP− and EAP+), the cryogenic main stage (EPC), and the upper composite. At ESA, the Ariane-5 model is used internally for the computation of initial loads, in support of the definition of payload structures during project feasibility studies. In this section, the Ariane-5 model will be used to compute

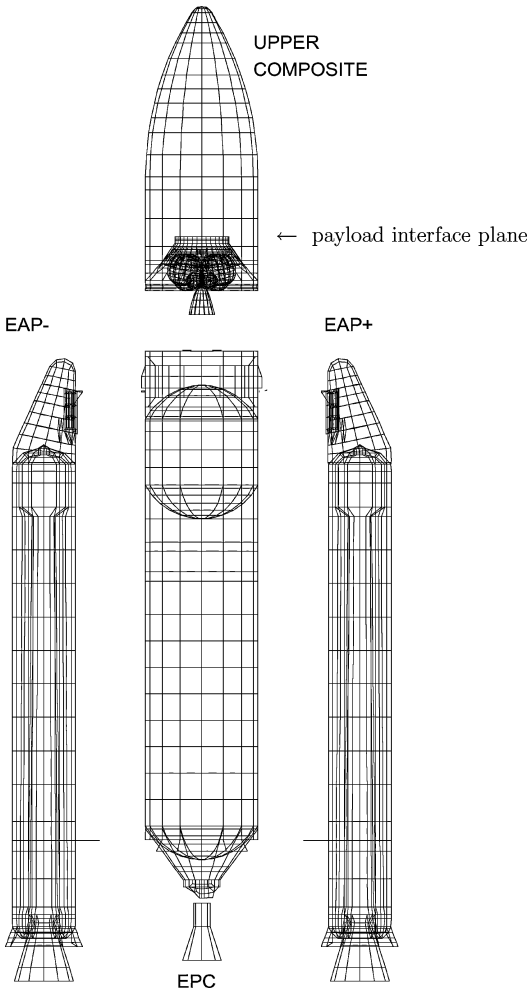

Fig. 7 Ariane-5 substructure FE models.

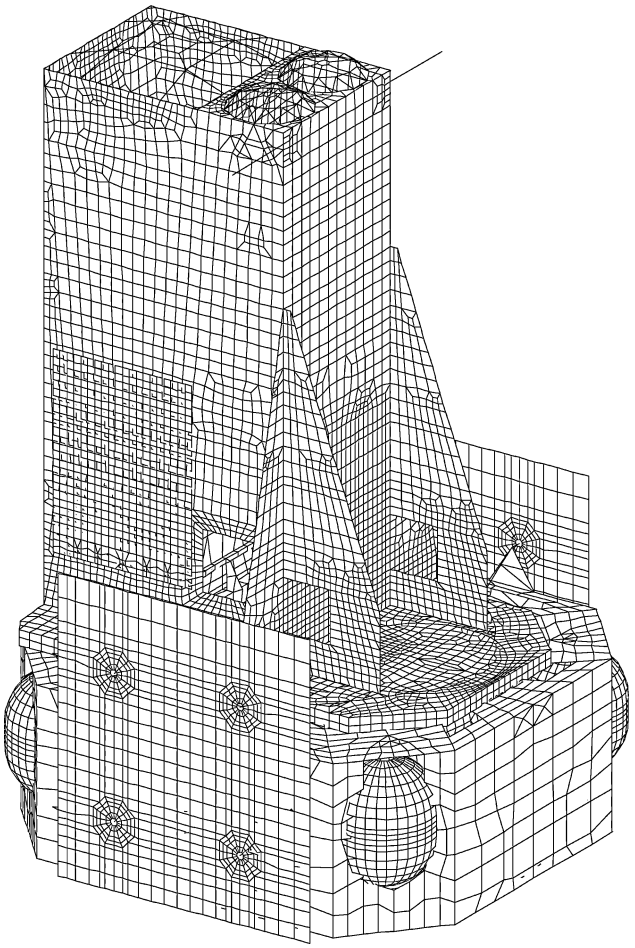

Fig. 8 Integral payload FE model (courtesy of Alenia Aerospazio).

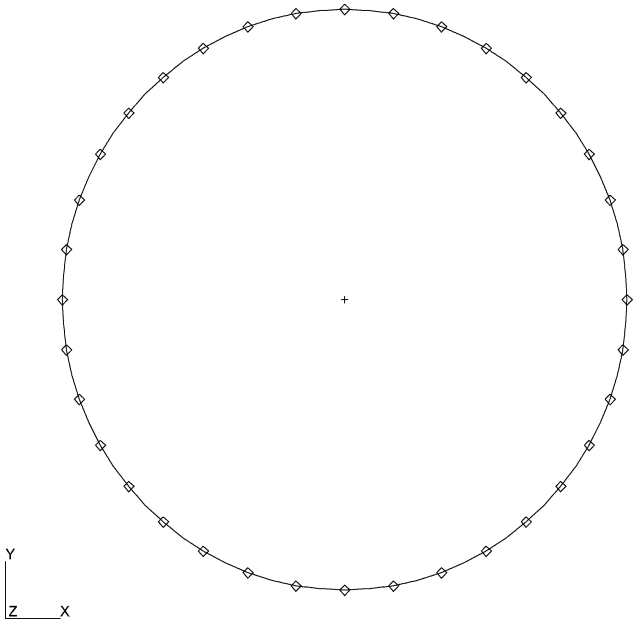

Fig. 9 Payload interface, 36 nodes.

a liftoff flight event. Usually the liftoff flight events start from a static condition whereby the launch vehicle sits on the launch pad. In that case, Earth gravity is explicitly needed for the simulation. Here, for reasons of simplicity, the liftoff flight event starts from a quasi-static equilibrium condition, where the free launcher has an initial acceleration that corresponds to the loads applied to the free system. Those loads are thrust forces, gravity, and lateral acoustic blastwave loads, similar to the loads defined when starting from the launch pad. As a consequence, the payload and launcher models are subject to internal loads during the liftoff flight event.

The payload FE model, that is, the Integral Satellite,[20] is shown in Fig. 8 and will be coupled to the payload interface under the fairing of the upper composite (Fig. 7). The payload model is reduced from approximately 120,000 DOF to 327 generalized DOF, comprising 216 interface DOF ($J = 216$), 6 generalized DOF associated with the rigid-body modes, 94 modal DOF ($P = 94$), and 11 MTA residual modal DOF ($N = 11$). The six DOF associated with the rigid-body modes are used to split absolute motion into rigid motion and flexible motion.[1,21] Because the payload FE model has a 36-node interface (216 DOF) to the Ariane-5 adapter, as shown in Fig. 9, the interface reduction method as outlined in Sec. VII was used to reduce the number of MTA pseudoeigenvectors associated with interface excitation from $J = 216$ to $B = 10$. In this procedure, the truncation frequency δ_t was chosen equal to ω_t, that is, $\delta_t = \omega_t = 100$ Hz [refer to Eq. (48)]. The 11th MTA vector is related to the gravity load $\tilde{F}_{ik}$ in Eq. (46), where $K = 1$. The total number of DOF for the complete Ariane-5/Integral CB system is approximately 800 DOF. The additional MTA pseudoeigenvectors, therefore, only imply an increase of 1.4% on the CB-system size. Note that the Ariane-5 substructures were reduced to classical CB substructures without the employment of MTA pseudoeigenvectors.

The transient analysis is computed in a direct way, that is, the Newmark time integration scheme is applied directly to the equations of motion without a modal decomposition in advance. The integration time step equates to 0.0002 s, and the time duration is 1.5 s. The output time step equates to 0.001 s, which yields a 250-Hz resolution (four time points needed per sine). The damping has been specified per substructure separately. For the payload model, a modal damping of 1% has been specified for all payload modes, including the MTA correction modes in the 100–306 Hz frequency range. The damping level of the MTA modes is set equal to the damping level that would have been assigned in this frequency range to the normal modes, if they would have been retained. This is in line with the damping strategy outlined in Sec. VI and is justified because the model has a rather fine mesh, which can adequately capture the high-frequency MTA pseudoeigenvectors.

The MD, MA, and MTA methods will now be employed to recover a stress inside the payload FE model. The equation for stress recovery according to the MD and MTA method is similar to Eq. (13) for displacement recovery because stress is a function of strain. For the MA method, the stress recovery equation is similar to Eq. (25). The objective is to quantify the difference between the MD response on the one hand and the MA and MTA responses on the other hand. The MD method is used to compute the reference solution. From the solution obtained with the MA and MTA methods, a quantifiable correction relative to the MD method can then be computed, if the number of fixed-interface normal modes for the payload substructure is kept constant. Note that a comparison of the MD, MA, and MTA responses with the FE-system response has not been attempted because of cost reasons.

The result for the axial stress in a bar element inside the payload FE model has been plotted in Figs. 10 and 11 for the MD/MA and the MD/MTA methods, respectively. The response curves for the MA and MTA methods are quite similar, especially for $t > 0.8$ s. For additional clarity, the differences $|\sigma_{\mathrm{MA}} - \sigma_{\mathrm{MD}}|$ and $|\sigma_{\mathrm{MTA}} - \sigma_{\mathrm{MD}}|$ have been plotted in Figs. 12 and 13, respectively. This difference can be regarded as the correction of the MA and MTA methods with respect to the MD method solution. The MA and MTA method stress corrections differ significantly for $t \leq 0.8$. In this part of the liftoff flight event, the loads are highly dynamic due to booster thrust variations and lateral acoustic blastwave excitation (high-frequency loads).

At $t = 0.35$ s, the correction of the MA and MTA methods amounts to 21.8 and 25.4%, respectively, of the MD method stress value (0.55 MPa). The highly dynamic loads require a dynamic correction as provided by the additional high-frequency MTA

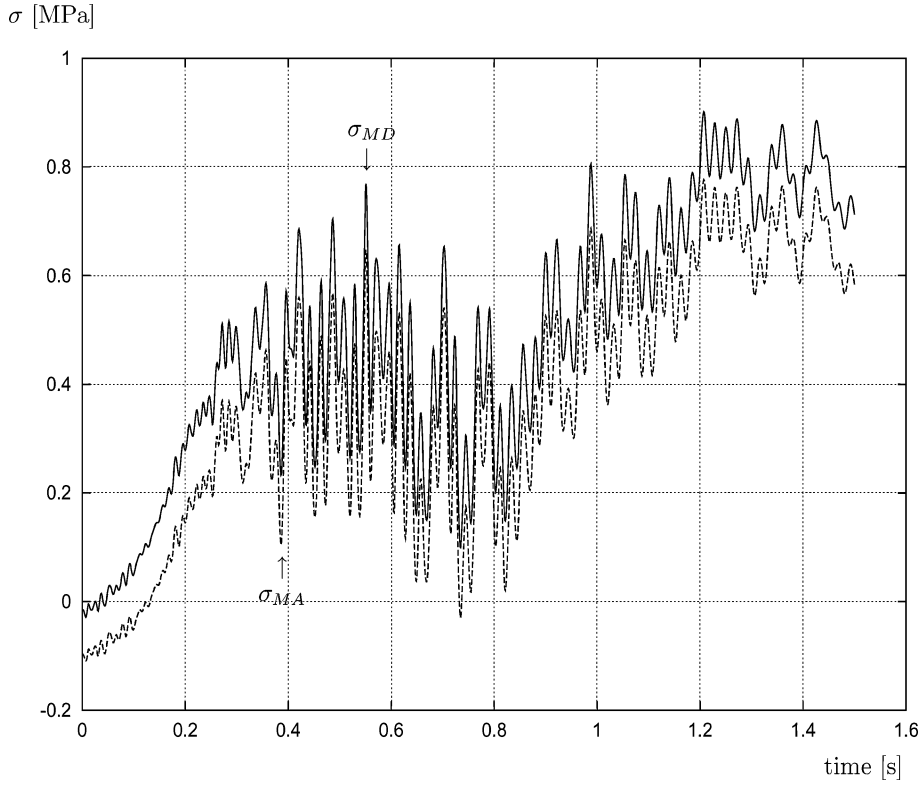

Fig. 10 Axial stress in bar element inside payload, MA vs MD.

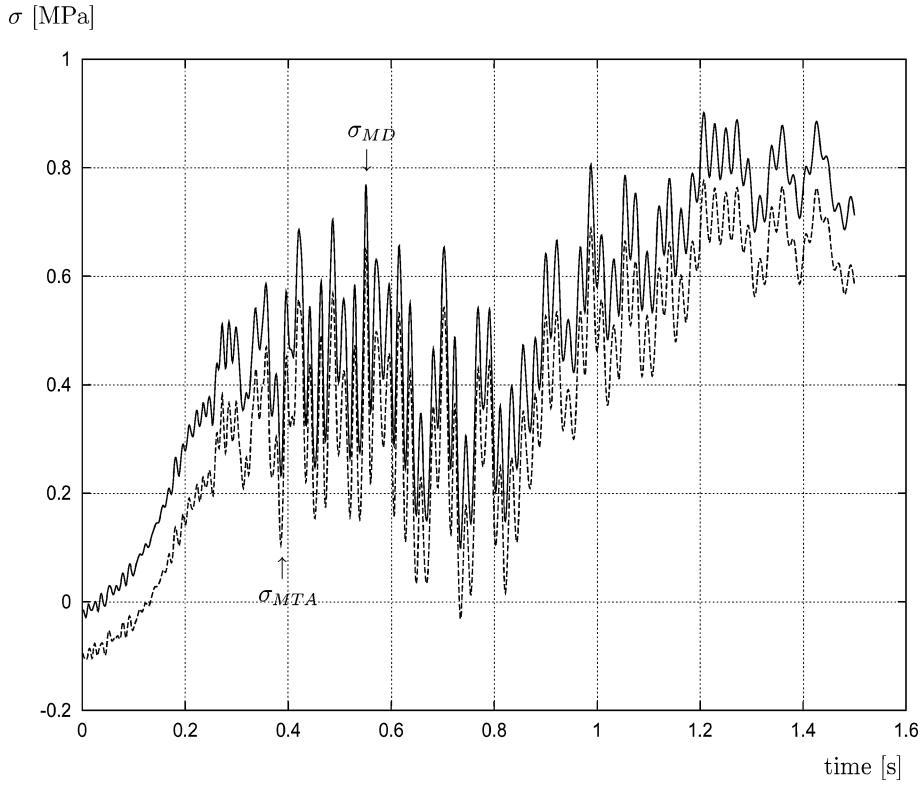

Fig. 11 Axial stress in bar element inside payload, MTA vs MD.

pseudoeigenmodes. For the last part of the analysis, the difference in correction diminishes because the high-frequency loads change into low-frequency loads. The total correction at the peak value ($t = 1.2$ s) for both methods is on the order of 14%. Obviously the difference between the MA and MTA methods will increase when a lower truncation frequency is chosen, as demonstrated in the example problems of Secs. VIII and IX. Still it can be seen from Figs. 12 and 13 that the MTA method correction contains more high-frequency dynamics because additional high-frequency pseudomodes have been included. The highest frequency observed in the MTA stress correction is about 100 Hz. Because the MTA pseudoeigenvectors are well represented by the payload model, and their 1% modal damping is thus justified, we can conclude that the MA method fails to model the high-frequency dynamics around 100 Hz. For high-frequency excitation, the MTA method is, therefore, more accurate.

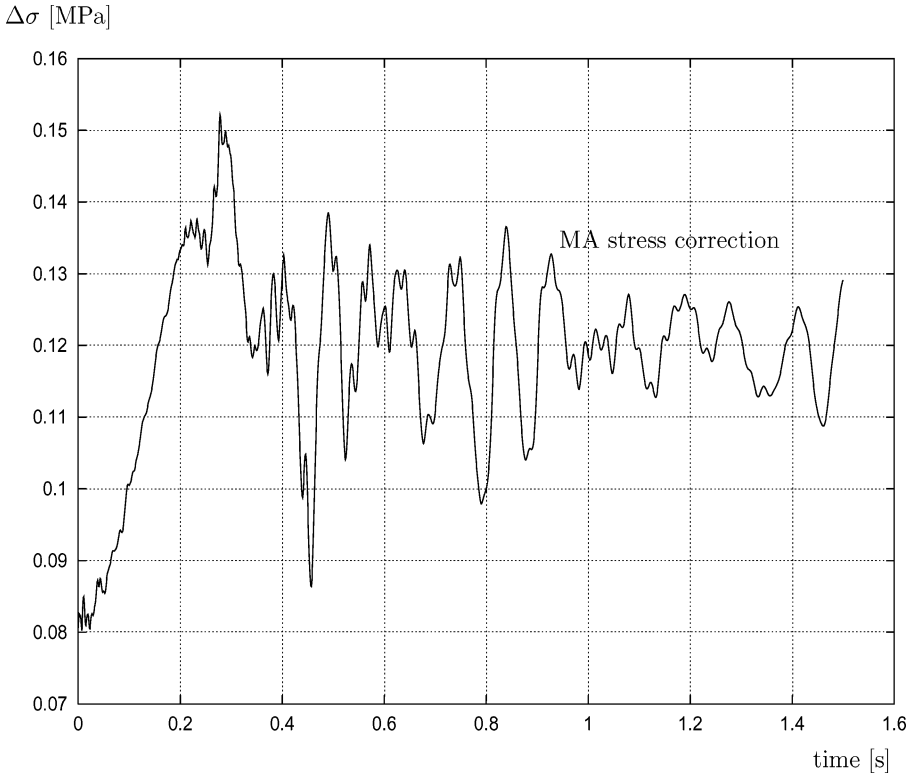

Fig. 12 MA stress correction relation relatives to MD method.

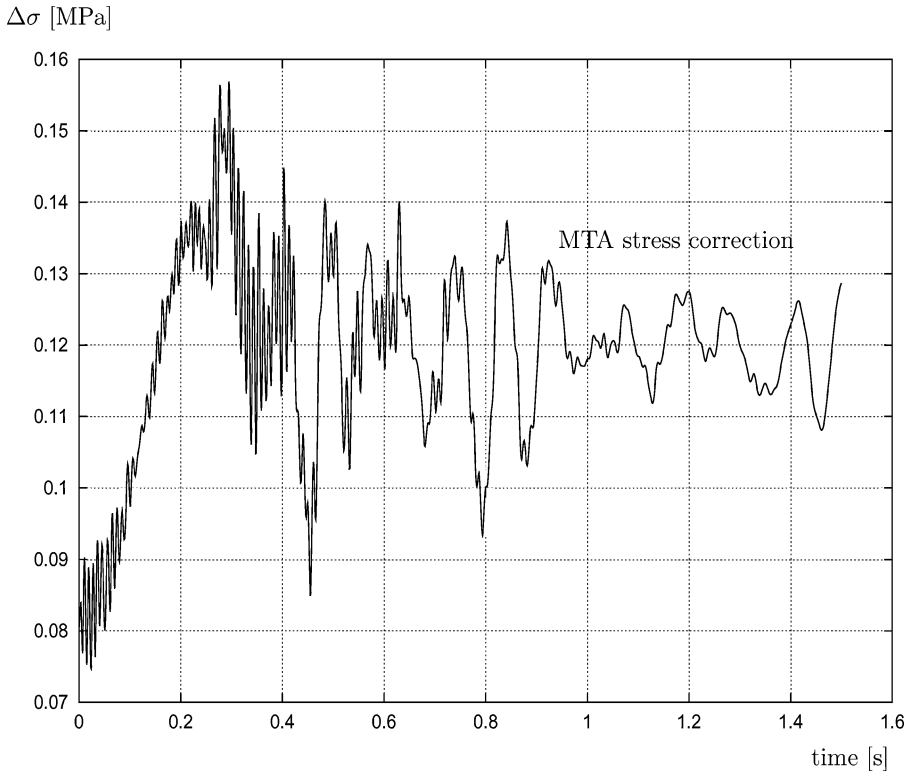

Fig. 13 MTA stress correction relation to MD method.

The frequency range of the correction modes is between 100 and 306 Hz. Hence, the apparent truncation frequency is about 306 Hz instead of 100 Hz, the actual truncation frequency of the CB model. Because the MTA method extends the validity of the model beyond the actual truncation frequency, as observed clearly in the beam example of Sec. VIII, one could decrease the actual truncation frequency, such that the apparent truncation frequency matches at least twice the highest frequency observed in the forcing function. Such strategies, which would make the MTA CB models very efficient, have not been explored in this paper but would certainly be worthwhile to investigate.

The MTA method, as outlined in this paper, could obviously also be used to recover the stresses in the Ariane-5 substructures. In that case, the internal loads would be composed of static gravity forces and possibly dynamic thrust forces and pressure forces, depending on the substructure considered.

XI. Conclusions

The MD, MA, and MTA methods have been employed for reduced dynamic substructure models with loads at the internal DOF of the corresponding FE model. For the MTA method, this led to an additional set of MTA pseudoeigenvectors, which are related to a set of spatial load distribution vectors, each containing correlated internal loads. In the classical MTA approach, the pseudoeigenvectors are related to interface excitation only. To make the MTA method more cost efficient for substructures with a high number of DOF at the interface, a method has been proposed to reduce the number of MTA pseudoeigenvectors using a flexible-interface reduction method.

By means of a simple beam example problem, it was demonstrated that the MTA method outperforms the conventional MD and MA methods in terms of accuracy, both in the frequency range of interest as well as beyond the truncation frequency. It was found that the additional set of MTA pseudoeigenvectors related to the internal loads improves the accuracy. When a more complex model of a space frame was used, it was also verified that for equal cost of computation (same number of modes) the MTA method performs best. Also in the latter example, loads were defined at the internal DOF of the substructures.

Finally, the MTA method was tested on large-scale payload model in an Ariane-5 coupled dynamic transient liftoff analysis. Gravity loads were applied to all internal DOF of the payload FE model. The correction relative to the MD method was found to be in the order of 25.4% when high-frequency booster thrust variations and blastwave loads excite the launcher. For the MA method, the correction was 21.8% at the same point in time. In the last part of the liftoff analysis (low-frequency loads), no significant difference between the MA and MTA method was obtained, in accord with expectations. Hence, it can be concluded that only in case of high-frequency excitation significant differences are found where the MTA method will be most accurate.

As concerns the recovery procedure, the MTA method is similar to the MD method. This implies that the amount of work associated with the recovery of displacements and displacement-related data is reduced as compared to the MA method. For reduced substructure models with internal loads, only one OTM is needed for the recovery of displacements instead of three. This means that with the MTA method a simple and accurate recovery procedure is available.

For CB models enriched with pseudoeigenvectors, the apparent truncation frequency is higher than the original truncation frequency. Therefore, it would be interesting to verify whether the actual truncation frequency can be decreased to reduce the number of retained modes and, hence, the dimension of the CB model.

Appendix: MA Method Static Correction

The eigenvalue problem, defined by Eq. (6), can also be written as follows when considering the full modal basis:

$$M_{ii}\varphi_{ii}\Lambda_{ii} - K_{ii}\varphi_{ii} = 0 \tag{A1}$$

Equation (A1) can also be written as

$$M_{ii}\varphi_{ii}\varphi_{ii}^T = K_{ii}\varphi_{ii}\Lambda_{ii}^{-1}\varphi_{ii}^T \tag{A2}$$

For mass-normalized modes, it follows that

$$G = K_{ii}^{-1} = \varphi_{ii}\Lambda_{ii}^{-1}\varphi_{ii}^T \tag{A3}$$

The total modal basis can be divided into kept modes φ_{ip} and deleted modes φ_{id}:

$$\varphi_{ii} = [\varphi_{ip} \quad \varphi_{id}] \tag{A4}$$

Then Eq. (A3) can be written as

$$G = G_p + G_d = \varphi_{ip}\Lambda_{pp}^{-1}\varphi_{ip}^T + \varphi_{id}\Lambda_{dd}^{-1}\varphi_{id}^T \tag{A5}$$

Hence, we find for the residual flexibility matrix

$$G_d = K_{ii}^{-1} - \varphi_{ip}\Lambda_{pp}^{-1}\varphi_{ip}^T = K_{ii}^{-1}\left[I - M_{ii}\varphi_{ip}\varphi_{ip}^T\right] \tag{A6}$$

Equation (A6) is equal to Eq. (28) in Sec. IV. When Eqs. (3), (13), and (14) are used, the internal displacements according to the MD method can be written as

$$\boldsymbol{x}_{i\mathrm{MD}} = \phi_{ij}\boldsymbol{x}_j + \varphi_{ip}\boldsymbol{q}_p \tag{A7}$$

Consequently, the internal accelerations (MD and MA method) are given by

$$\ddot{\boldsymbol{x}}_i = \phi_{ij}\ddot{\boldsymbol{x}}_j + \varphi_{ip}\ddot{\boldsymbol{q}}_p \tag{A8}$$

From the second row partition of Eq. (7), the modal accelerations $\ddot{\boldsymbol{q}}_p$ can be found:

$$\ddot{\boldsymbol{q}}_p = \varphi_{ip}^T\boldsymbol{F}_i - \varphi_{ip}^T(M_{ij} + M_{ii}\phi_{ij})\ddot{\boldsymbol{x}}_j - \Lambda_{pp}\boldsymbol{q}_p \tag{A9}$$

Substitution of Eq. (A9) into Eq. (A8) gives

$$\ddot{\boldsymbol{x}}_i = \phi_{ij}\ddot{\boldsymbol{x}}_j + \varphi_{ip}\varphi_{ip}^T\boldsymbol{F}_i - \varphi_{ip}\varphi_{ip}^T(M_{ij} + M_{ii}\phi_{ij})\ddot{\boldsymbol{x}}_j - \varphi_{ip}\Lambda_{pp}\boldsymbol{q}_p \tag{A10}$$

From here it can be easily verified that substitution of Eq. (A10) into Eq. (18) of Sec. IV, as well as the subsequent use of Eqs. (A6) and (A7), leads to Eq. (27) in Sec. IV:

$$\boldsymbol{x}_{i\mathrm{MA}} = \boldsymbol{x}_{i\mathrm{MD}} + G_d\left\{\boldsymbol{F}_i - \left[M_{ij} - M_{ii}K_{ii}^{-1}K_{ij}\right]\ddot{\boldsymbol{x}}_j\right\} \tag{A11}$$

Acknowledgments

The author gratefully acknowledges the valuable discussions with D. J. Rixen of the Delft University of Technology. In addition the author acknowledges the support of T. K. Henriksen of the ESA.

References

[1]Hurty, W. C., "Dynamic Analysis of Structural Systems Using Component Mode Synthesis," *AIAA Journal*, Vol. 3, No. 4, 1965, pp. 678–685.

[2]Craig, R. R., and Bampton, M. C. C., "Coupling of Substructures for Dynamic Analysis," *AIAA Journal,* Vol. 6, No. 7, 1968, pp. 1313–1319.

[3]Rayleigh, J. W. S., *The Theory of Sound*, 2nd ed., Vol. 1, Dover, New York, 1896, Chap. 5, p. 100.

[4]Williams, D. E., "Dynamic Loads in Aeroplanes Under Given Impulsive Loads with Particular Refererence to Landing and Gust Loads on a Flying Boat," Royal Aircraft Establishment, TR SME 3309 and 3316, 1945.

[5]Craig, R. R., *Structural Dynamics, An Introduction to Computer Methods*, Wiley, New York, 1981, pp. 350, 351, 478–480.

[6]Fransen, S. H. J. A., "An Overview and Comparison of OTM Formulations on the Basis of the Mode Displacement Method and the Mode Acceleration Method," Worldwide Aerospace Conf. & Technology Showcase, MSC.Software Corp., 2002, Paper 17, URL: http://www.mscsoftware.com/events/aero2002.

[7]Fransen, S. H. J. A., and Bellini, M., "Structural Verification of the Columbus Payload Racks by Means of Coupled Loads Analysis," *European Conference on Spacecraft Structures, Materials & Mechanical Testing* [CD-ROM], CNES/ESA/DLR/ASI, 2002.

[8]Dickens, J. M., Nakagawa, J. M., and Wittbrodt, M. J., "A Critique of Mode Acceleration and Modal Truncation Augmentation Methods for Modal Response Analysis," *Computers and Structures*, Vol. 62, No. 6, 1997, pp. 985–998.

[9]Dickens, J. M., and Stroeve, A., "Modal Truncation Vectors for Reduced Dynamic Substructure Models," AIAA Paper 2000-1578, April 2000.

[10]Rixen, D. J., "Generalized Mode Acceleration Methods and Modal Truncation Augmentation," AIAA Paper 2001-1300, April 2001.

[11]MacNeal, H. H., "A Hybrid Method of Component Mode Synthesis," *Computers and Structures*, Vol. 1, 1971, pp. 581–601.

[12]Rubin, S., "Improved Component-Mode Representation for Structural Dynamic Analysis," *AIAA Journal*, Vol. 13, No. 8, 1975, pp. 995–1006.

[13]Guyan, R. J., "Reduction of Stiffness and Mass Matrices," *AIAA Journal*, Vol. 3, No. 2, 1965, p. 380.

[14]Craig, R. R., "Coupling of Substructures for Dynamic Analyses: An Overview," AIAA Paper 2000-1573, April 2000.

[15]Rixen, D. J., "High Order Static Correction Modes for Component Mode Synthesis," *Fifth World Congress on Computational Mechanics*, Vienna Univ. of Technology, Vienna, 2002, Paper 80915.
[16]Craig, R. R., and Chang, C. J., "Substructure Coupling for Dynamic Analysis and Testing," NASA CR-2871, Feb. 1977.
[17]Tan, Y.-C., Castanier, M. P., and Pierre, C., "Characteristic-Mode-Based Component Modes Synthesis for Power Flow Analysis in Complex Structures," AIAA Paper 2000-1470, April 2000.
[18]Castanier, M. P., Tan, Y.-C., and Pierre, C., "Characteristic Constraint Modes for Component Modes Synthesis," *AIAA Journal*, Vol. 39, No. 6, 2001, pp. 1182–1187.
[19]Kilroy, K., *Quick Reference Guide—MSC.Nastran Version 2001*, MSC.Software Corp., Los Angeles, 2001.
[20]Notarnicola, M., Paron, A., Tizzani, L., and Evans, E., "INTEGRAL—Structural Mathematical Model Description and Dynamic Analysis Results," Space Div., TR INT-TN-AI-0089, Issue 2, Alenia Aerospazio, Turin, Italy, April 1998.
[21]Kreis, A., "Analysis of Prestressed Free Bodies," Technical Rept., Kreis Consultancies, Pragg-Jenaz, Switzerland, May 1992.

C. Pierre
Associate Editor

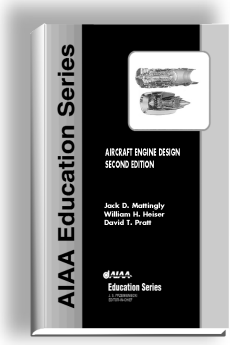

AIRCRAFT ENGINE DESIGN, SECOND EDITION

Jack D. Mattingly—University of Washington • William H. Heiser—U.S. Air Force Academy • David T. Pratt—University of Washington

This text presents a complete and realistic aircraft engine design experience. From the request for proposal for a new aircraft to the final engine layout, the book provides the concepts and procedures required for the entire process. It is a significantly expanded and modernized version of the best selling first edition that emphasizes recent developments impacting engine design such as theta break/throttle ratio, life management, controls, and stealth. The key steps of the process are detailed in ten chapters that encompass aircraft constraint analysis, aircraft mission analysis, engine parametric (design point) analysis, engine performance (off-design) analysis, engine installation drag and sizing, and the design of inlets, fans, compressors, main combustors, turbines, afterburners, and exhaust nozzles.

The AEDsys software that accompanies the text provides comprehensive computational support for every design step. The software has been carefully integrated with the text to enhance both the learning process and productivity, and allows effortless transfer between British Engineering and SI units. The AEDsys software is furnished on CD and runs in the Windows operating system on PC-compatible systems. A user's manual is provided with the software, along with the complete data files used for the Air-to-Air Fighter and Global Range Airlifter design examples of the book.

2002, 692 pp, Hardback
ISBN: 1-56347-538-3
List Price: $95.95
AIAA Member Price: $69.95

Contents:
- The Design Process
- Constraint Analysis
- Mission Analysis
- Engine Selection: Parametric Cycle Analysis
- Engine Selection: Performance Cycle Analysis
- Sizing the Engine: Installed Performance
- Engine Component Design: Global and Interface Quantities
- Engine Component Design: Rotating Turbomachinery
- Engine Component Design: Combustion Systems
- Engine Component Design: Inlets and Exhaust Nozzles
- Appendices

American Institute of Aeronautics and Astronautics
Publications Customer Service, P.O. Box 960, Herndon, VA 20172-0960
Fax: 703/661-1501 • Phone: 800/682-2422 • E-mail: warehouse@aiaa.org
Order 24 hours a day at www.aiaa.org

AIAA
American Institute of Aeronautics and Astronautics

02-0545